AFRL-AFOSR-VA-TR-2020-0047

The effect of high altitude environments on the dislocation structure evolution during fatigue cracking of legacy and next generation aerospace aluminum alloys

James Burns
UNIVERSITY OF VIRGINIA

11/18/2019
Final Report

Air Force Research Laboratory
AF Office Of Scientific Research (AFOSR)/ RTA1
Arlington, Virginia 22203
Air Force Materiel Command

REPORT DOCUMENTATION PAGE

Form Approved
OMB No. 0704-0188

1. REPORT DATE *(DD-MM-YYYY)*	2. REPORT TYPE	3. DATES COVERED *(From - To)*
21-05-2020	Final Performance	15 Aug 2016 to 14 Aug 2019

4. TITLE AND SUBTITLE
The effect of high altitude environments on the dislocation structure evolution during fatigue cracking of legacy and next generation aerospace aluminum alloys

5a. CONTRACT NUMBER

5b. GRANT NUMBER
FA9550-16-1-0211

5c. PROGRAM ELEMENT NUMBER
61102F

6. AUTHOR(S)
James Burns

5d. PROJECT NUMBER

5e. TASK NUMBER

5f. WORK UNIT NUMBER

7. PERFORMING ORGANIZATION NAME(S) AND ADDRESS(ES)
UNIVERSITY OF VIRGINIA
1001 N EMMET ST
CHARLOTTESVILLE, VA 22903-4833 US

8. PERFORMING ORGANIZATION REPORT NUMBER

9. SPONSORING/MONITORING AGENCY NAME(S) AND ADDRESS(ES)
AF Office of Scientific Research
875 N. Randolph St. Room 3112
Arlington, VA 22203

10. SPONSOR/MONITOR'S ACRONYM(S)
AFRL/AFOSR RTA1

11. SPONSOR/MONITOR'S REPORT NUMBER(S)
AFRL-AFOSR-VA-TR-2020-0047

12. DISTRIBUTION/AVAILABILITY STATEMENT
A DISTRIBUTION UNLIMITED: PB Public Release

13. SUPPLEMENTARY NOTES

14. ABSTRACT
Next generation structural integrity management of airframe fatigue damage can increase accuracy and reduce overconservatism
by coupling the substantial progress in understanding and modeling mechanical loading spectra with similar efforts to capture the strong influence of an environmental spectrum. Recent efforts have quantitatively demonstrated orders of magnitude reductions in the fatigue crack growth rates (da/dN) for testing in high altitude environments (e.g. low temperature and low water vapor pressure (PH2O)) pertinent to high altitude flight. Critically, despite a constant exposure parameter (PH2O/frequency), differences in da/dN are observed between tests at 23C and low temperature environments (below -30C). The main objective of this project is to gain an understanding of the factors governing the environmental cracking behavior via characterization of the dislocation structure in the near crack wake regime of an aerospace Al alloy (7075-T651) at different environmental conditions. This study will develop and employ a novel multi-scale characterization technique implementing high resolution-electron backscatter diffraction (HR-EBSD) using cross-correlation techniques, focused ion beam (FIB) lift-out for sample preparation used for transmission electron microscopy (TEM) to characterize local damage structure in the fatigue crack wake. Work has been done to find the best practice for the cross-correlation analysis of the EBSD data, and TEM sample preparation to prevent unintended material microstructure changes due to sample preparation. This multi-scale characterization technique was used to get initial results to gain insights into rigorously defining the mechanistic understanding of the fatigue cracking as it occurs in a high altitude environment. More specifically, how the localized damage proximate to the crack wake surface changes as a function of tem

15. SUBJECT TERMS
Fatique Cracking, dislocation structures, high altitude structurual behavior

16. SECURITY CLASSIFICATION OF:			17. LIMITATION OF ABSTRACT	18. NUMBER OF PAGES	19a. NAME OF RESPONSIBLE PERSON
a. REPORT	b. ABSTRACT	c. THIS PAGE			TILEY, JAIMIE
Unclassified	Unclassified	Unclassified	UU		19b. TELEPHONE NUMBER *(Include area code)* 703-588-8316

The effect of high altitude environments on the dislocation structure evolution during fatigue cracking of legacy and next generation aerospace aluminum alloys

James T. Burns, Adam W. Thompson

University of Virginia

Abstract:

Next generation structural integrity management of airframe fatigue damage can increase accuracy and reduce over-conservatism by coupling the substantial progress in understanding and modeling mechanical loading spectra with similar efforts to capture the strong influence of an environmental spectrum. Recent efforts have quantitatively demonstrated orders of magnitude reductions in the fatigue crack growth rates (da/dN) for testing in high altitude environments (e.g. low temperature and low water vapor pressure (P_{H2O})) pertinent to high altitude flight. Critically, despite a constant exposure parameter (P_{H2O}/frequency), differences in da/dN are observed between tests at 23°C and low temperature environments (below -30°C). The main objective of this project is to gain an understanding of the factors governing the environmental cracking behavior via characterization of the dislocation structure in the near crack wake regime of an aerospace Al alloy (7075-T651) at different environmental conditions. This study will develop and employ a novel multi-scale characterization technique implementing high resolution-electron backscatter diffraction (HR-EBSD) using cross-correlation techniques, focused ion beam (FIB) lift-out for sample preparation used for transmission electron microscopy (TEM) to characterize local damage structure in the fatigue crack wake. Work has been done to find the best practice for the cross-correlation analysis of the EBSD data, and TEM sample preparation to prevent unintended material microstructure changes due to sample preparation. This multi-scale characterization technique was used to get initial results to gain insights into rigorously defining the mechanistic understanding of the fatigue cracking as it occurs in a high altitude environment. More specifically, how the localized damage proximate to the crack wake surface changes as a function of temperature given a constant P_{H2O}/frequency.

Introduction:

The aerospace industry commonly uses aluminum alloys for fabrication of a wide variety of airframe components due to the materials ease of fabrication and its high strength to weight ratio; the most common aluminum alloys used in aircraft being the 7xxx and 2xxx series.[1] Despite these alloys high strength they are susceptible to the most common cause of damage on aircraft, which is fatigue[2,3] The airframe structural management community commonly applies linear elastic fracture mechanics (LEFM) to model crack extension via the fundamental principle of similitude, where a constant growth rate is expected for a given stress intensity range (ΔK), which relates the applied load, crack length and the specimen geometry to get the magnitude of the elastic stress field.[4] This correlation of ΔK to the growth kinetics of the advancing crack front (da/dN) allows for a similitude between laboratory specimens and in service parts. What LEFM does not take into account is how the crack growth rates are effected by the cracking environment.

It is well known that the fatigue crack growth behavior of aluminum is effected by the environment it is being cracked in, specifically moist environments where these effects are attributed to a phenomena known as hydrogen embrittlement or hydrogen assisted cracking. Specifically, of importance to the aerospace industry is how high altitude (10,000 feet or higher) environment effects fatigue behavior as a significant amount of loading events occur for some of the parts found on aircraft that are subjected to cyclic loading in a high altitude environment.[5] There is two major differences in a high altitude environment when compared to normal laboratory environment and they are a lower partial pressure of water (P_{H2O}) and lower temperatures. Studies of fatigue cracking in low water vapor pressure environments show expectantly lower crack growth rates occur as the amount of water available decreases, this is understood by a decrease in the hydrogen available in the environment yields less hydrogen in the sample lessening the effect of hydrogen assisted cracking[6–11]. While other studies looking at fatigue cracking in aluminum added in the low temperature environments which show a drop in fatigue crack growth rates at similar water vapor pressure levels but lower temperatures, which is attributed to the reduction of water vapor pressure in equilibrium with the ice that forms on the material as well as a reduction of hydrogen diffusion kinetics or the effect of the crystallographic crack path[12–17]. The knowledge gap that exists in the literature is the lack of data which decouples the effects of hydrogen and temperature on fatigue in aluminum as well as getting at the underlining mechanism to why these crack growth rates are observed in high altitude environments.

The overarching goal of this study is increase the understanding of this phenomenon to enable incorporation of these environmental effects into next generation LEFM life prediction approaches. This could potentially reduce the inspection burden on aircraft by justifying life extensions on certain parts, increase the availability of the aircraft for flight by validating the increase in time between inspections, as well as possibly leading to new component designs or new alloy development to mitigate the fatigue damage that has always plagued the aerospace industry. In order to achieve this overarching goal a there are several knowledge gaps that need to be better understood:

1. Data needs to be collected in a variety of high altitude environments (pertinent temperature and P_{H2O} ranges) at the full range of ΔK, as well as studies done to ensure the experimental protocol to get the data is rigorous and provides similitude.
2. Either new LEFM software needs to be developed or existing LEFM software needs to be updated to incorporate the effects the environment has on fatigue cracking to better predict fatigue life times for aerospace components.
3. Rigorously define the mechanistic understanding of the fatigue cracking as it occurs in these high altitude environments.

This study addresses the issue of rigorously defining the mechanistic understanding of the fatigue cracking as it occurs in a high altitude environment. The goal of this study is to develop a novel and rigorous multi-scale characterization method using EBSD, HR-EBSD, and FIB/TEM to gain insights into the mechanistic understanding of the fatigue cracking in high altitude environments. Additionally, this study will apply this method to targeted fatigue test to provide insights into the mechanistic understanding of the fatigue cracking of aluminum in high altitude environments.

Results:

Task 1: Develop multi-scale method to characterize the local damage structure of a fractured specimen.

The initial task of this research was to establish and validate a novel multi-scale characterization method that will be used to characterize the local damage structure of a fractured material and to ensure the rigorous isolation of the variables of interest. Robertson et. al.[18,19] has employed focused ion beam (FIB) lift-out and transmission electron microscopy (TEM) to evaluate dislocation structure determine the governing mechanisms of the crack. Alternately, Wilkinson et. al.[20] have used high resolution-electron backscatter diffraction (EBSD) and cross-correlation techniques to characterize crack wake dislocation structures (using the OpenXY software[21]). Despite the power and utility of both of these characterization techniques there are critical short-comings in the application of these techniques to date. Most basically, both TEM and HR-EBSD are used to analyze the damage structure in the sub-100 nm scale typically taken from individual grains with indifference to the grain orientations themselves. By failing to control the grains orientation it is not possible to determine if observed differences in the damage structure are due to (1) the independent variable of interest (i.e. environment, microstructure, loading conditions, etc.) or (2) simple differences in the grain orientation relative to the primary loading axis and surrounding grains. Resolving these issues will enable the correlation of the information received from the EBSD and TEM analysis about the fatigue damage which so far has been insufficiently studied. Our six step novel multi-scale method combines the techniques of HR-EBSD and TEM providing the fidelity of TEM with the field of view of HR-EBSD all the while allowing for the targeting of a specific ΔK and a specific grain orientation. Each step of the multi-scale method is outlined in Figure 1, where the additional details for the steps are highlighted as:

Step 2: Perform a fracture mechanics test at the environmental parameters of interest. Identify the location in the crack wake that corresponds to a given constant ΔK between samples to enable control of that variable. Then excise the sample from that specific location.

Step 2: To get a surface prepared for EBSD it is best practice to finish the polishing by utilization of an argon ion mill. The maximum size samples that can fit into the chamber of the ion mill is 20 mm in length, 20 mm in width and 5 mm in height, but most fracture specimens begin significantly larger than this thus it generally needs to be polished or cut down to the appropriate size. Since any alteration of the materials microstructure is undesired for the fractured surface areas under investigation it was imperative to find the depth of the damage that would be caused by the saw cuts to the material, which was done as a part of task 2 and is described there.

Step 3: The big concern for this step was undesired microstructure alteration from the possible re-crystallization that could occur from the ion milling itself via the energy of the ion beam or from the heating of the sample from the ion mill process. Due to the configuration of the sample holder for the ion mill the sample has to be mounted with an adhesive, such as Crystalbond 509, which has a softening temperature of 71°C, because of this the limiting temperature of the sample was set at $\approx$ 60°C to insure the integrity of the adhesive preventing undesired milling to occur from the sample shifting in the soften adhesive. From a report given by the manufacture of

the ion mill a temperature of about 60°C is reached at the sample after ≈ two hours of ion milling. Using two hours as the maximum length of time of milling, test were run with the maximum accelerating voltage of the ion mill and it was determine that no recrystallization occurred during the two hour mill to the ion milled surface, which the details of this confirmation are listed in task 2. Additionally, it should be noted that 60°C is conservatively about 13% of the melting temperature of 7xxx series aluminum[22]. Using the previously described ion mill and time settings it was important to optimize the width dimension of the samples, and it was determined that optimal range for the width dimension for aluminum was between 1 and 0.5 mm. The ion mill was unable to completely mill the width of the sample when larger than 1 mm and with widths below 0.5 mm the ion mill left more rounding on the exiting edge as well as having less usable area for EBSD analysis due to the "rounding" of the milled surface from the milling process. This width range is fairly uniform where denser materials like the monel should be polished to the 0.5 mm mark and materials less dense than the 7xxx series aluminum can be left closer to the 1 mm mark. For best practices it was determined that the fractured specimens should be saw cut to about 5 mm below the fractured surface and have a final length of about 15 mm (gives safe space due to imprecision of the saw cut), giving the sample an initial size of about 15 mm in length, 5 mm in width and 7.6 mm in height. To polish the sample down to the required dimensions required a polishing method to be developed to minimize the damage caused by the mechanical polishing process, which is described in detail in task 2.

Step 4: A special holder for the SEM was designed to hold the samples and it was determined best practice to have the fractured edge of the samples facing down as it gave better results closer to the fractured edge and didn't give "false" solutions on the edge of the sample due to signal coming from deeper within the sample. A global EBSD scan was done on all of the ion milled surface near the crack wake surface to determine the orientation of all of the grains at the fractured surface and the total area of the EBSD scans were about 1 mm across x 0.5 mm deep.

Step 5: Experiments were done to determine the resolution limit of the detector for HR-EBSD, which was determined to be 100 nm. This resolution limit was also used as the minimum step size set for the HR-EBSD scans to maximize the area that can be analyzed in a given amount of time while insuring that the maximum amount of information could be obtained from the sample. The grains of interest, which were previously selected for HR-EBSD were performed with a scan area of about 50 μm x 50 μm and the data from the HR-EBSD scans were analyzed using cross-correlation software named, CrossCourt, to characterize the crack wake dislocation structures. Heat maps of total geometrically necessary dislocations (GND) density and kernel averaged misorientation (KAM) were generated and qualitatively examined to determine the level of deformation as well as the character of the deformation observed in the area.

Step 6: The TEM sample preparation began with selecting a Pt protection layer protocol which was systematically researched to obtain the best practice to deploy this protocol. The details of this research are laid out in task 2, but the protocol that best mitigated the surface damage to the TEM sample was the combination of first depositing an electron-beam Pt layer using a 5 KeV accelerating voltage and 1.6 nA beam current to a depth of ≈ 110 nm and then finishing the layer with a deposition of ion-beam platinum using a 30 KeV accelerating voltage and a beam current

around 90 pA where the final dimensions of the Pt layer were about 10.50 μm long by 2.25 μm wide and 2.00 μm deep. After the deposition layer was complete on the edge of the fatigue crack wake surface that was exposed during the ion-mill step, the next step was to create a modified lift-out method that could be utilized for the TEM sample required for this new characterization method. A pattern of three boxes were ion milled around the observed platinum strip with the dimensions of the boxes being: Box 1 & 3: 2.00 μm long, 5.83 μm wide and 33.00 μm deep. Box 2: 18.50 μm long, 4.75 μm wide and 33.00 μm deep. These boxes were positioned around the Pt strip at an equiaxed distance with a slightly larger distance on the right side to allow for a "landing pad" for the nano-manipulator to attach to the sample. A nano-manipulator was attached to the "landing pad" on the sample followed by a final extraction cut being performed about 6 μm below the fractured surface. The sample was extracted and welded to a TEM finger grid where it was thinned down to a final thickness of less than 150 nm thick but thicker than 100 nm. These steps for the FIB preparation are outlined in Figure 2. The thinned sample is then observed in the TEM on the zone axis of the EBSD determined orientation of the grain, using brightfield STEM (BF-STEM). Images are taken at optimized tilts near the zone axis allowing for a more complete image of the local deformation structure ideal for qualitative analysis.

This novel multi-scale characterization method was demonstrated on a fractured single edge notched tension (SENT) specimen of nickel-copper alloy (Monel K-500). This demonstration illustrates the importance in selecting a constant grain orientation when making comparisons of the local damage structure as well as a major pitfall that can occur when analyzing the local damage structure via EBSD and TEM. For this SENT specimen the entire cracked area was fit in the ion mill target area. This allowed for EBSD to be collected and analyzed for the entire cracked area, which is shown in Figure 3. Also highlighted in Figure 3 are the three chosen grains for HR-EBSD and TEM data collection and analysis, which are of different grain orientations, but all have the relatively same driving force value, K ranged from 43 MPa$\sqrt{m}$ to 45 MPa$\sqrt{m}$. The differences observed in Figure 4, of the deformation observed when comparing samples of different grain orientations was expected despite having a similar driving force as previous study done by Wert et. al shows how the deformation evolution is different when comparing multiple grains with different orientations.[23] Figure 4 results highlight the importance of holding the grain orientation constant when trying to make comparisons in damage structure from grain to grain, however this demonstration also shows consideration of the crystallographic orientation or sample tilt relative to the electron beam needs also to be considered when doing the EBSD and TEM data collection. Figure 5, shows a collection of TEM images taken from one of the samples where three different crystallographic alignment protocols were used; (1) crystallographic alignment relative to the TEM electron beam is the same as it was originally for EBSD/HR-EBSD data collection, (2) crystallographic alignment set to the zone axis of the sample obtained from the center area of the sample and left in this orientation for all TEM images collected, and (3) the crystallographic alignment was set to the zone axis obtained from the area of the sample where the individual images were collected. From this data in Figure 4, it is shown that using the same sample taken with the same grain orientation can yield three different conclusions to the local damage structure observed in the TEM images based on which of the widely accepted protocols chosen for the analysis. It is considered best practice to use the crystallographic alignment relative to the TEM electron beam in the same position it was originally

for EBSD/HR-EBSD data collection, therefore allowing for a direct comparison between the HR-EBSD and TEM data.

Task 1 has demonstrated the need for and determined a set protocol to rigorously examine the local damage structure of the crack wake area. Additional to holding the crack driving force and grain orientation constant, special consideration to the crystallographic orientation for not only the grains being compared but also for the sample orientation relative to the electron beam used for TEM image collection. It should be noted that the demonstration was done on the material monel instead of the AA7075-T651 because of the issues differentiating the damage from the rolling process during the manufacturing of the material and the deformation that arose from the fracturing of the specimen while analyzing the HR-EBSD data.

Future work planned for this task is to develop a protocol to quantitatively analyze the local damage as a function of depth from the crack wake surface. Future experiments are planned to aid the work to differentiate the damage created from the rolling process during and the deformation that arose from the fracturing of the specimen for analysis of the HR-EBSD data for the AA7075-T651 material. The future experiments planned to differentiate these deformations will also examine the possibility of some of the deformation created from the cracking process is relieved as the crack tip passes. Furthermore, more work needs to be done for the validation of the HR-EBSD data collected via comparison of local damage substructure data obtained using FIB/TEM data collected to confirm the consistency in the deformation observed.

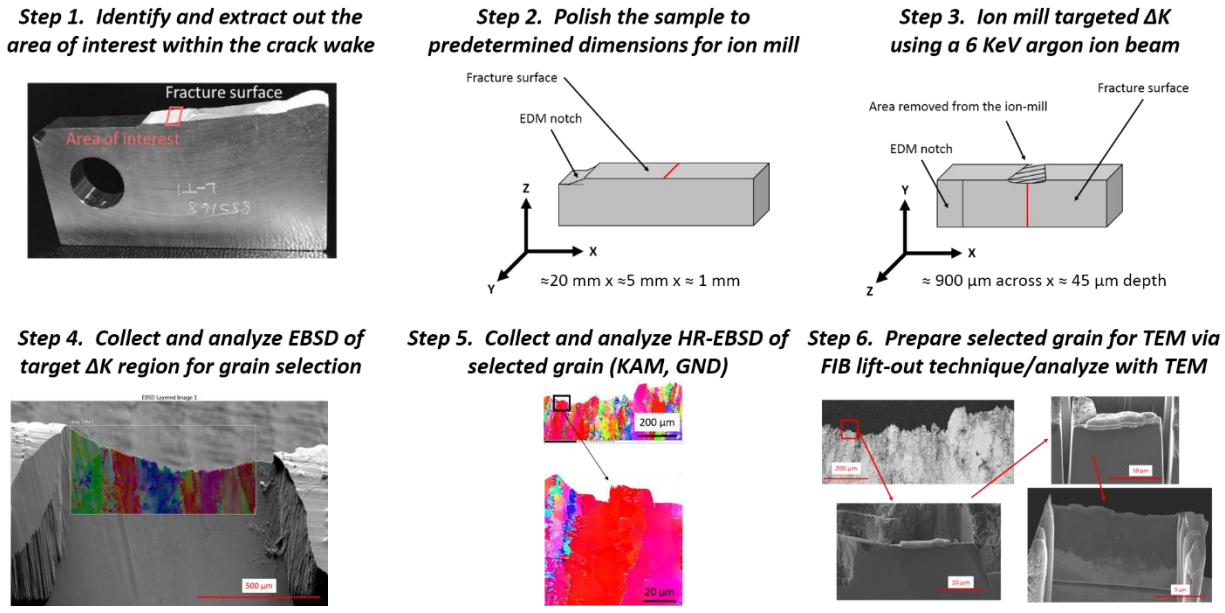

Figure 1 – A step by step overview the novel multi-scale characterization method, which employees the use of EBSD and FIB/TEM.

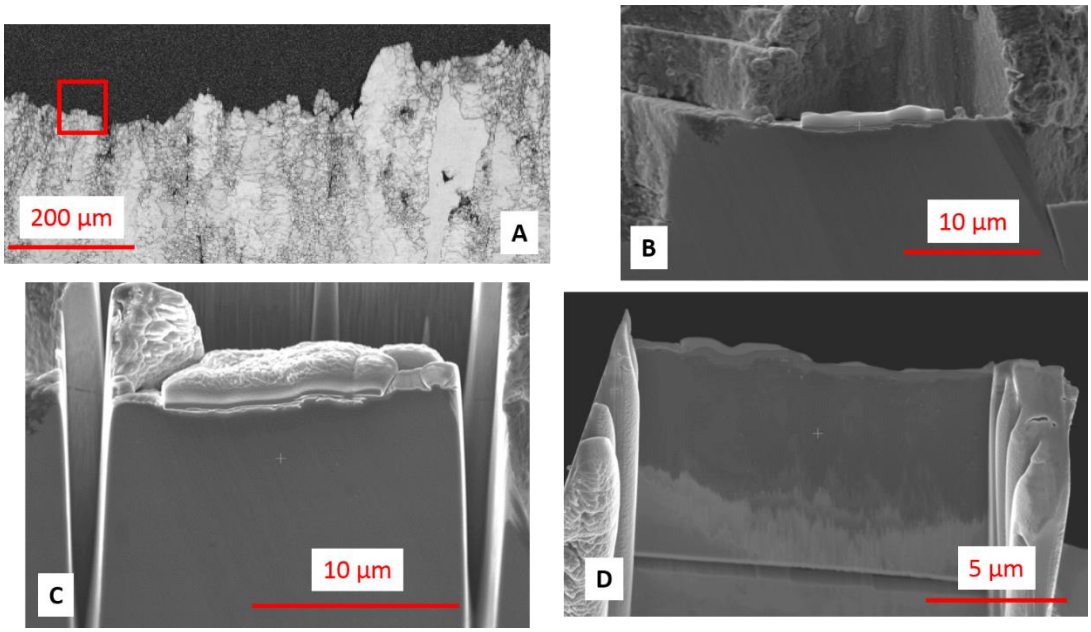

Figure 2 – A) An image of the EBSD scanned area where the area of interest is outlined in the red box. B) The Pt protection layer on the area of interest that will be lifted-out for TEM analysis. C) The area of interest after the trench milling done by the 3 box pattern. D) The final sample thinned to about 150 nm in thickness.

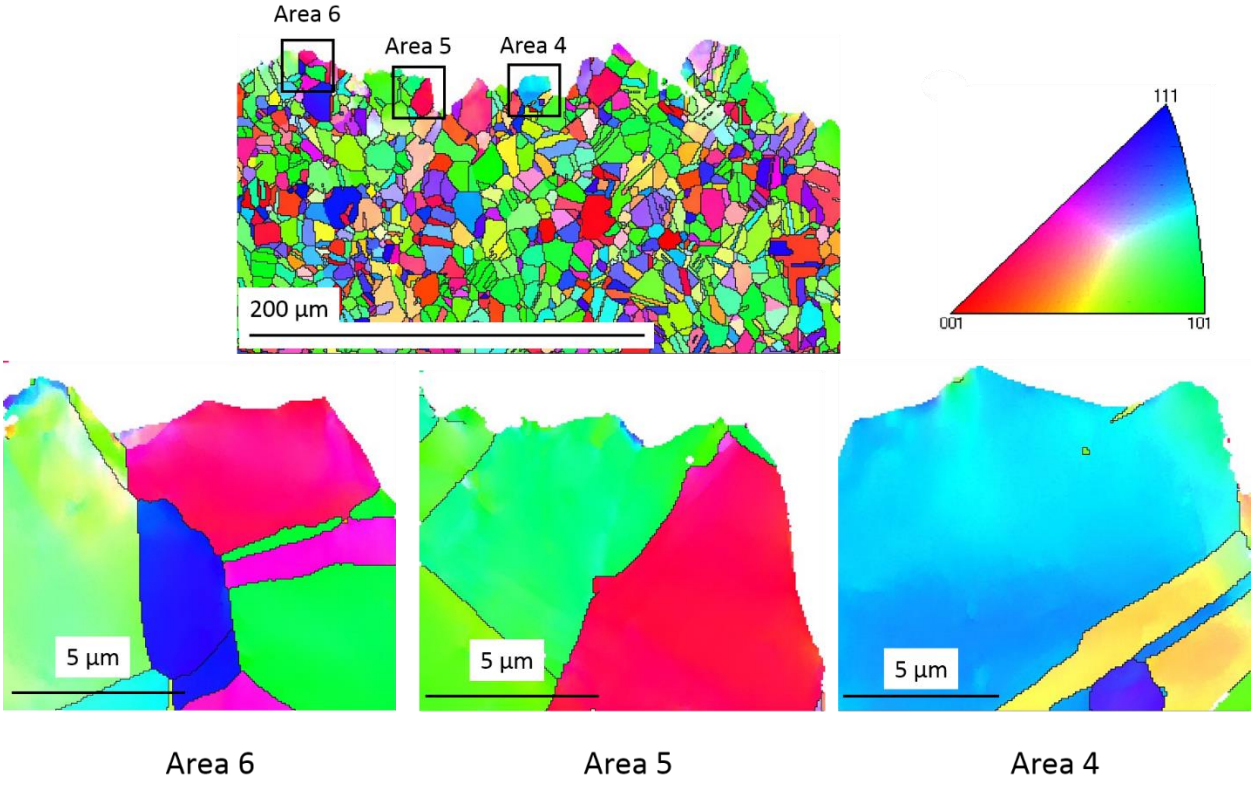

Figure 3 – Global EBSD data collected of the fracture with the three areas selected for HR-EBSD and TEM analysis. Areas 4, 5, and 6 have relatively the same K but different crystal orientations, where area 4 is (212), area 5 is (414), and area 6 is (114).

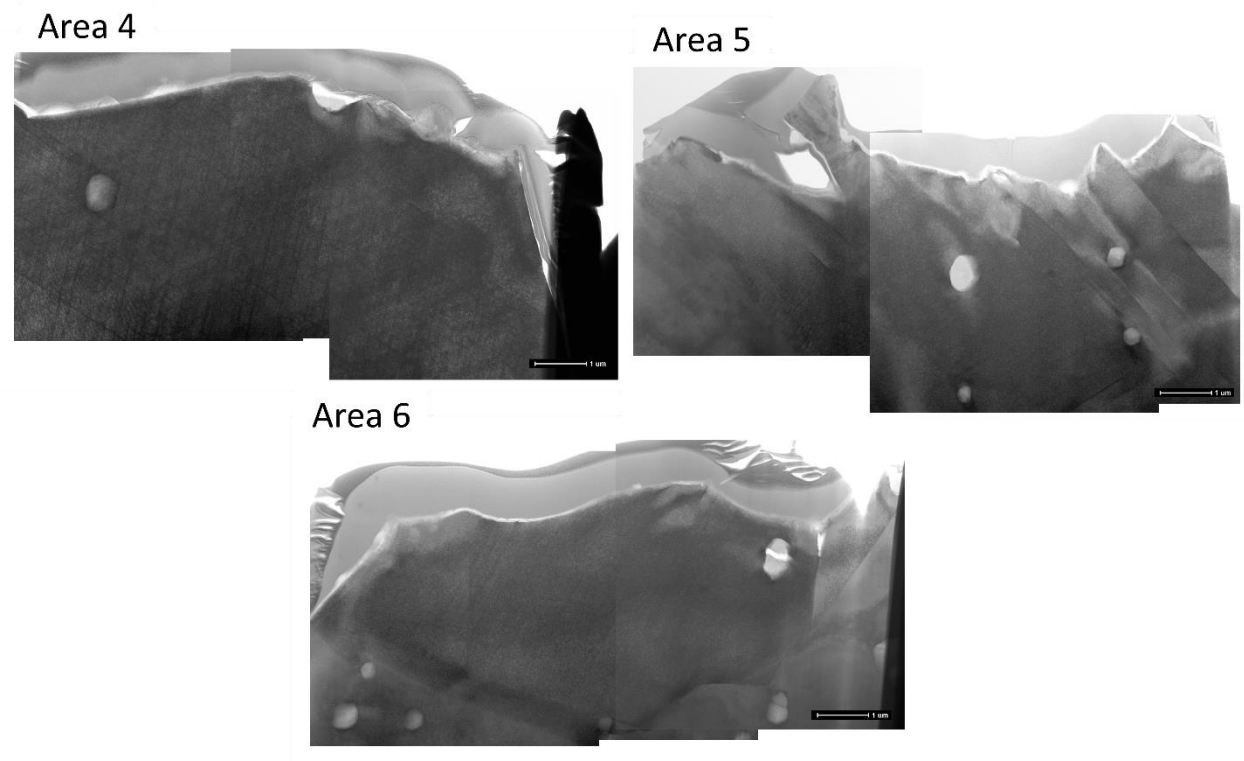

Figure 4 – Stitched TEM images of the three samples (areas 4, 5, and 6). TEM images were taken at a magnification of 14,000x with the sample in a crystallographic alignment set to the zone axis of the sample, which was obtained from the center area of the TEM sample and left in this orientation for all TEM images collected.

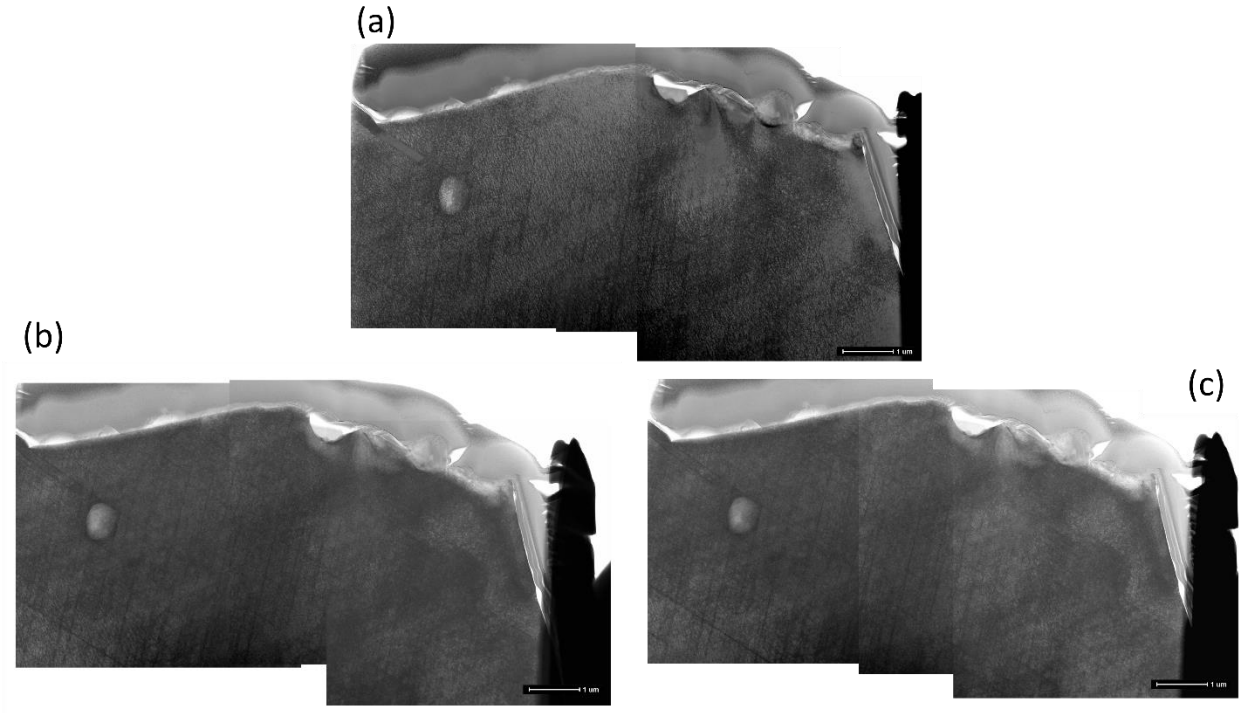

Figure 5 – A collection of TEM images taken and stitched together from area 4, showing the three different crystallographic alignment protocols; (a) crystallographic alignment relative to the TEM electron beam is the same as it was originally for EBSD/HR-EBSD data collection, (b) crystallographic alignment set to the zone axis of the sample obtained from the center area of the sample and left in this orientation for all TEM images collected, (c) the crystallographic alignment was set to the zone axis obtained from the area of the sample where the individual images were collected.

Task 2: Evaluate the role of sample preparation damage accumulated in the sample used for the multi-scale method.

Many of the steps described in task 1 were informed by the experiments and data that was collected in task 2. While all sample preparation techniques used during the multi-scale characterization method has the potential to alter the microstructure of the material in a negative way it is important to note that studies done previous utilizing TEM analysis suffers from the lack of examination of the protection layer deposition to reduce the undesirable influence on the local damage structure near the surface of the FIB lift-out sample[7,18,24]. This damage to the surface of the sample during FIB preparation as well as the sample preparation from the previous steps all could obfuscate quantitative and qualitative characterization of the local damage structure from the near crack wake area. Details of the evaluation of the role sample preparation damage accumulated in the sample used for this multi-scale characterization method are highlighted as such:

Step 1: To extract the sample out of the initial cracked specimen required a high speed sectioning blade, which does cause alteration to the materials microstructure via deformation and heat. Since any alteration of the materials microstructure is undesired for the fractured surface areas under investigation it was imperative to find the depth of the damage that would be caused by the saw cuts to material. From subsequent testing it was determined that the saw caused about 225 μm of damage, and with a factor of safety it was determined best practice to keep the saw cuts at least 500 μm away from any desired area for microstructure analysis.

Step 2: As stated before best practices determined that the fractured specimens should be saw cut to about 5 mm below the fractured surface and have a final length of about 15 mm, giving the sample an initial size of about 15 mm in length, 5 mm in width and 7.6 mm in height. To polish the height down to the required 5 mm a polishing method was developed to minimize the damage caused by the mechanical polishing. The first step to this minimization of the sample preparation damage effecting the analysis was determining the amount of depth of material that is removed from the ion milled surface. From light microscope observations of test samples it was determined that the ion mill removed about 40 microns of the polished surface. This provided a base line for the level of finish that was required as the final polishing step could not induce more than 40 microns of damage in depth. The manufacturers of the grinding paper and polishing solutions provided the size of the particles and then a factor of safety (three times the size of the particles) was put into place to insure that all mechanical polishing damage would be removed from the ion mill process. To polish the width down to the required range of 1 to 0.5 mm it was determined that the finer the polished surface was the less surface roughness was observed, where the surface roughness was determined to cause an uneven finish to the ion mill surface, thus the same polishing method developed to minimize the damage caused by mechanical polishing for the height was employed to do the same for the width dimension. Best practice was determined to be all polishing steps be finished using a 1 μm diamond slurry, where at this level the damage would be adequately removed from the ion mill process as well as being the coarsest particle size to be used where it didn't cause the ion mill process to leave an uneven finish. Additionally, it was determined that the settings used for the ion mill process didn't recrystallize the ion milled surface

which was confirmed via EBSD analysis as well as a comparison TEM sample prepared from a location at a significant distance from the ion-milled surface.

Step 6: To best practice for the deposition of a Pt protection layer was determined by a published study, which was designed to test four different Pt protection layer protocols, where the best practice would be the one that minimized the surface damage to the prepared TEM sample. The area of interest was a small section of bulk AA7075-T651 where the surface was cut with a high speed saw for the purpose of simulating a deformed surface observed with a fatigue crack wake surface. The surface damage caused by the Pt protection layer protocol was analyzed via BF-TEM utilizing the FIB lift-out method for sample preparation. The protection layer deposition protocols examined were:

1. **Current best practices:** a deposition layer of ion-beam platinum using the common ion-beam setting of 30 KeV (accelerating voltage) and 90 pA (beam current).
2. **Method developed by May Martin to limit the damage caused by the ion-beam deposition**[25]**:** a deposition layer of ion-beam platinum using 30 KeV and 50 pA for the first half of the deposition depth (0.5 μm) and then finish the deposition depth using the ion- beam condition used by the current best practices (30 KeV and 90 pA).
3. **Low current:** a deposition layer of ion-beam platinum using the lowest practical beam current setting for the given FIB tool, which was done at 30 KeV and 26 pA.
4. **Electron-beam/Ion-beam combination**: a deposition layer of electron-beam platinum using 10 KeV and 0.54 nA to a depth of ≈ 50 nm[7] and then finished with a deposition of ion-beam platinum using the beam conditions outlined by the current best practices.

The protocol determined to best at mitigating the surface damage to the TEM sample was the electron-beam/Ion-beam combination. Although it was the best protocol observed in this study further observations from the TEM analysis showed the recommended depth of electron beam deposition of platinum recommended by the manufacturer of the FIB tool was not the optimal depth of E-beam Pt[26]. Additionally, the effects of heating caused by the platinum deposition process where inconclusive, so another test using a 5th protocol was developed to optimize the E-beam platinum deposition depth, and to observe adverse effects from heating of the sample during the deposition protocol. The 5th deposition protocol was done on a different piece of bulk AA7075-T651 where the sample was cold rolled to about 50% of the original thickness to significantly increase the amount of deformation in the material. The surface of the sample was then polished to remove the recrystallization layer created from the adiabatic heating as well as other surface abnormalities during the cold working process. The 5th deposition protocol was:

5. **Optimized electron-beam/ion-beam combination**: a deposition layer of electron-beam platinum using 5 KeV and 1.6 nA to a depth of ≈ 110 nm and then finished with a deposition of ion-beam platinum using the beam conditions defined by the current best practices from protocol #1.

The results of this sample yielded a better protocol for the deposition of the platinum protection layer as not only was the surface damage all but eliminated, but no adverse effects from heating of the sample during the deposition were observed. This results of this study on the FIB induced damage during platinum deposition in the near surface region of AA7075-T651 was published in the Micron journal volume 118 in 2019.

Task 2 has rigorously evaluated the role of sample preparation damage accumulated in the sample used for the multi-scale method. In this task all sample preparation techniques have been optimized to mitigate the damage created from the process allowing for the rigorous analysis to be performed via EBSD and TEM without the complications of sample preparation alterations to the examined areas.

Future work for this task is planned to do a similar examination of the Pt layer deposition with a Xe ion source, utilized by a new group of tools called plasma-focused ion beam (P-FIB), rather than the traditional Ga ion source utilized by the FIB. Characterization facilities are moving to P-FIB rather than the traditional Ga source FIB due to the negative side effect of Ga implantation into the material possibly creating intermetallic materials and altering the original microstructure of the material[27]. A thorough examination of the Xe ion induced damage during platinum deposition in the near surface region hasn't been done to date in literature and should be examined to determine if the best practice shown from the study by Thompson et. al.[28] for Ga ion FIBs can be used by Xe P-FIBs or if a new Pt deposition protocol is needed.

Task 3: Apply the multi-scale method to inform high altitude environment fatigue behavior.

This task aims to specifically answer the question, "Does the fatigue behavior shown in the data in Figure 6, which shows fatigue tests performed at a constant P_{H2O}/f but different temperatures (specifically above and below -30°C) having different fatigue crack growth rates for AA7075-T651 despite having similar driving force at the fatigue crack tip correlate with changes in the crack wake damage structure?"

With tasks 1 & 2 complete a novel and rigorous multi-scale characterization method has been developed with the best practices determined. Task 3 sought to apply this characterization method to inform the operative mechanisms for high altitude environment fatigue behavior, specifically examining the question, "Does the fatigue behavior shown in the data in Figure 6, which shows fatigue tests performed at a constant P_{H2O}/f but different temperatures (specifically above and below -30°C) having different fatigue crack growth rates for AA7075-T651 despite having similar driving force at the fatigue crack tip correlate with changes in the crack wake damage structure?" To address this question two separate fatigue test were run each in an environment where the P_{H2O}/f was equal to 0.027 Pa·s but one was fatigue cracked at room temperature (around 23°C) and the other at a temperature of -65°C. Two different ΔK values were selected, one at a ΔK of 9 MPa√m representing the Paris regime where the crack growth rates are similar at both temperatures, and one at a ΔK of 6 MPa√m representing the near-threshold regime where a clear deviation in crack growth rates is observed in the two different temperatures in the da/dN vs. ΔK charts found in Figure 6. Using the data the crack lengths where these values of ΔK could be found on the crack wake surface were identified via light microscope images (Figure 7) and the areas were extracted as described in task 1. The areas of interest were polished to the dimensions described in task 1, were ion milled yielding two ion mill areas on both samples. The areas of interest were then analyzed using EBSD to identify the orientations of the grains in the ion milled area. A {001} grain was chosen for each of the four areas for further HR-EBSD analysis because AA7075-T651 has a cubic texture from the rolling process which makes a {001} grain orientation likely to be found on every ion mill location made for this study. The chosen grains for HR-EBSD and TEM analysis are highlighted on the EBSD data for each of the four locations in Figure 8. The HR-EBSD data was analyzed using CrossCourt software and GND density heat maps and KAM maps were generated (Figures 9 & 10). The four locations were then lifted-out as described in task 1 and examined in the TEM using BF-STEM, where the images collected for each of the locations can be seen in Figure 11. During the qualitative analysis of the BF-STEM images to gain insights into what differences in the local damage structure may exist, a layer noticeably different from the bulk was observed near the surface of each of the sample examined, which can be seen in the BF-STEM images in Figure 12. Additional diffraction analysis was done on this layer, which is shown in Figure 13 to further provide insights into what difference could possibly exist in the local damage structure.

In conclusion the main goal of Task 3 was to gain insights into the local damage structure for two fatigue specimens that were both cracked in a 0.027 Pa·s environment with one cracked at room temperature around 23°C and the other cracked at a temperature of -65°C, where in the near threshold regime a noticeable deviation in crack growth rates was observed. Both the GND density maps and the KAM maps (Figures 9 & 10) generated from the HR-EBSD data show the

deformation to be significantly more localized than the estimated cyclic plastic zone size predicted by LEFM. Additionally, both the GND density maps as well as the KAM maps show the large amounts of residual deformation that was introduced during the rolling process. This residual deformation shows up most prominently in the random pockets of heavy deformation far from the crack wake surface, which obfuscates deformation evolution of the local damage structure as well as determining the differences in the near threshold regime samples. Furthermore, no clear gradient as a function of depth from the crack wake surface appears in any of the samples. Analysis of the BF-STEM images suggests the dislocation structure development for both temperatures in the ΔK of 9 MPa√m samples is similar, but in the ΔK of 6 MPa√m samples we see a clear difference as we see dislocation structure in the room temperature sample but no dislocation structure development in the -65°C, which this difference seems to correlate with the observed differences in the growth rates for these samples. This data suggest a possible temperature dependent restriction of dislocation organization and/or an effect on the H-dislocation interaction. As stated previously an observed "recrystallized" layer appeared in all four samples analyzed, but appeared to be more uniform in thickness for the room temperature samples and more of a globular look for the -65°C samples. This layer was formed by either. One, in front of the crack tip (the plastic zone) the crystal structure for this orientation, experiences plastically induced rotation allowing for the fatigue crack to continue to grow on a more energetically favorable plane. Two, the energy produced in the plastic zone in front of the crack front is sufficient enough to cause dynamic recrystallization to occur orientating the crystal structure for a more energetically favorable plane as well as clearing the fatigue crack path from precipitates and other obstacles that would inhibit fatigue crack growth from occurring.

From the diffraction analysis shown in Figure 13, it shows that for the two ΔK of 9 MPa√m samples that at best little or no plastically induced rotation or dynamic recrystallization has occurred at this point in the crack wake surface as indicated by the comparison of the diffraction pattern taken from the bulk of the sample to the diffraction patterns that were taken from the near surface of the samples. Here is it shown that for the -65°C sample the bulk grain orientation and the near surface orientation are almost the same and for the room temperature sample the small difference observed in the two diffraction patterns could have come from a slight rotation or a nearby precipitate. The most compelling data is observed with the ΔK of 6 MPa√m samples where the near surface orientation diffraction pattern for the room temperature sample shows a complete change in crystallographic orientation, but it can't be determined from this data if this occurred from dynamic recrystallization or plastically induced rotation and when compared to the -65°C sample, which is clearly different observation is made, which is similar to the ΔK of 9 MPa√m samples. Just as the dislocation structure evolution suggests the diffraction analysis also suggest the possibility of a temperature dependence on the crystallographic orientation change that is driven by the advancing fatigue crack front to plastically induce rotation and/or dynamic recrystallization that may be assisted by the presence of hydrogen whose effects are also dependent on temperature.

Future work for this task is to further develop a mechanistic understanding of the temperature dependent fatigue behavior, despite having a P_{H2O}/f. To do so more work is needed provide the insights needed to develop the understanding desired. It starts with continuing the work to answer the question posed in Task 3. Specifically, data shows that for temperatures below -30° C tests performed at constant P_{H2O}/f but different temperatures show different growth rates for AA7075-T651, does this behavior correlate with changes in the crack wake dislocation structure? To answer this question is to continue examining the "recrystallized layer that was

observed in all four samples. A qualitative difference was observed between the samples cracked at -65°C and room temperature and further diffraction analysis suggest a complete change in crystal orientation for the {100} grains fatigue cracked at a near-threshold ΔK value at room temperature with a 0.027 Pa·s environment, but these same grains in the same conditions only changing the temperature from about 23°C to -65°C seem to slow down or stop this rotation of the orientation. This behavior correlated with what was observed in the da/dN vs. ΔK for the fatigue crack growth rates, which justifies further evaluation. This further evaluation need will be fulfilled using a transmission EBSD (T-EBSD) technique done in the TEM which is referred to as ASTARS. The HR-EBSD analysis is limited to a 100 nm step size which inhibits its ability to adequately examine the "recrystallized" layer, whereas the ASTARS will be able to analyze the "recrystallized" layer at step size of 25 nm enabling for a more thorough investigation. What will be looked for is possible evidence of micro or nano sized grains in the layer, which would suggest some dynamic recrystallization occurred changing the original crystal structure to be more energetically favorable or a gradient of crystal orientation change from the original orientation to the other observed orientation near the crack wake surface, which would suggest plastically induced rotation of the crystal. Furthermore, other questions need to be addressed to fully examine this unexplained behavior. First, is there a change in the local crack tip plasticity evolution/dislocation structure/local damage structure for AA7075-T651 tested in UHV at 23° C, -30°C and -65°C? By fully removing the environment in all cases this effort will eliminate any possible role of hydrogen and specifically investigate the role of temperature on the local damage structure. The same characterization will be performed at the same two ΔK values to investigate how the applied load influences this behavior at the given temperatures completely absent of hydrogen. Second, how does the local damage structure change as a function of loading frequency for 7075-T651 in UHV at -65° C? Either a strong frequency dependence or frequency independent behavior will provide critical insights. If the dislocation structure changes with loading frequency then this implies that the local crack tip process (recovery, dislocation motion, etc.) is time dependent, thus a strong influence of temperature, independent of H. If the dislocation structure does not change, then this opens up the use of loading frequency as a critical variable to decouple the relative influence of temperature dependent dislocation motion and H-diffusion. Specifically, testing at a constant P_{H2O} value either set by the vacuum system at 23° C or by low temperature could be performed with systematically varying frequency. Consistent behavior between the low and high temperature experiments would suggest that temperature dependent H diffusion is not controlling. Third, to what extend does the different bulk slip behavior associated with 7075-T651 (wavy) and 2199-T86 (planar) influence the crack wake dislocation structure at UHV and at intermediate temperatures/P_{H2O}? Do the same trends observed from Question 1-2 hold true for 2199-T86? While the bulk slip behavior is different the diffusivities are expected to be similar so this comparison will help to differentiate between mechanisms.

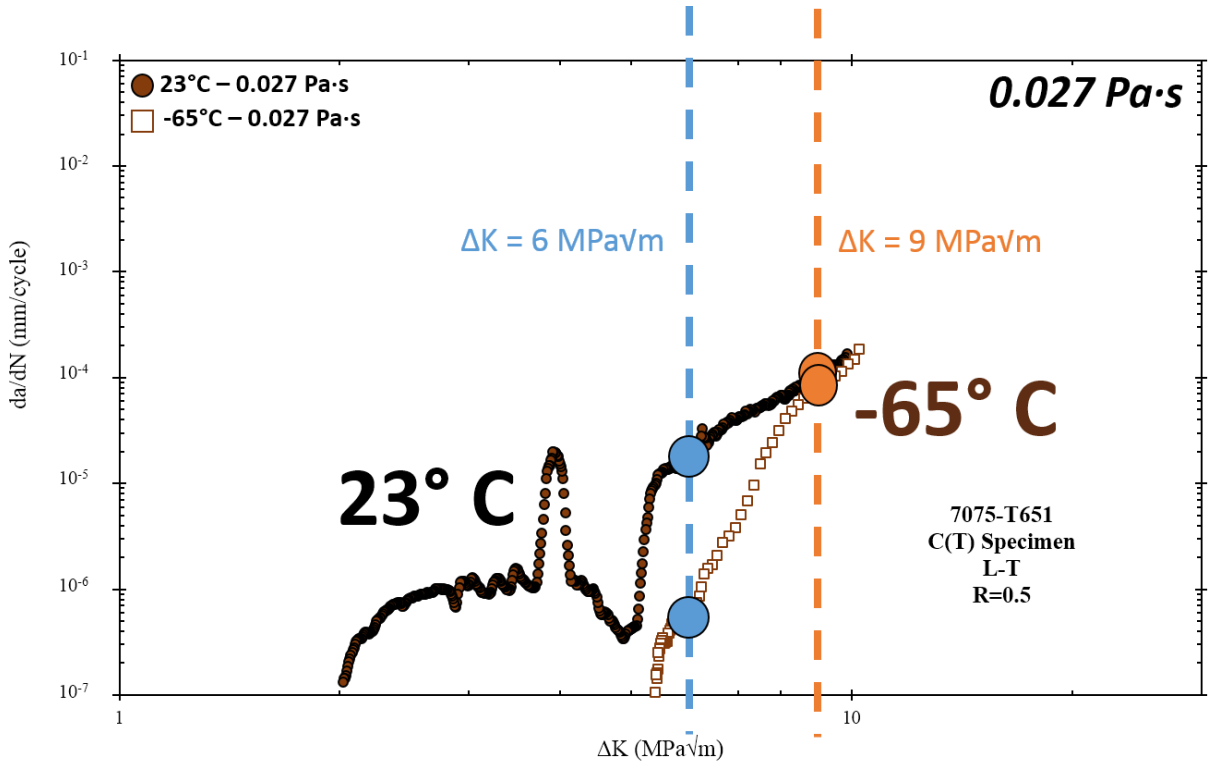

Figure 6 – da/dN vs. ΔK charts of two different fatigue test where both were run in an environment with a P_{H2O}/f value of 0.027 Pa·s, but one of them of the test was run at room temperature around 23°C and the other was run at a temperature of -65°C.

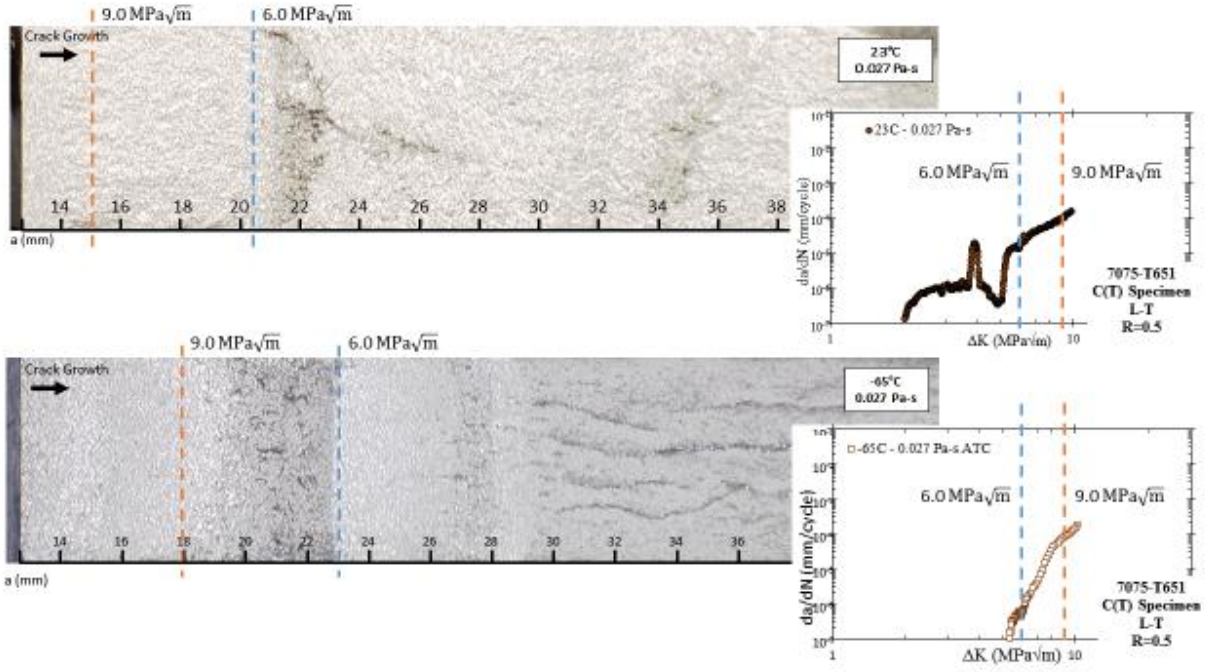

Figure 7 – Light microscope images of the crack wake surface for both of the fatigued samples where the areas of the samples containing the ΔK of 6 MPa√m and 9 MPa√m are highlighted on both the corresponding da/dN vs. ΔK chart as well as the crack wake surface image.

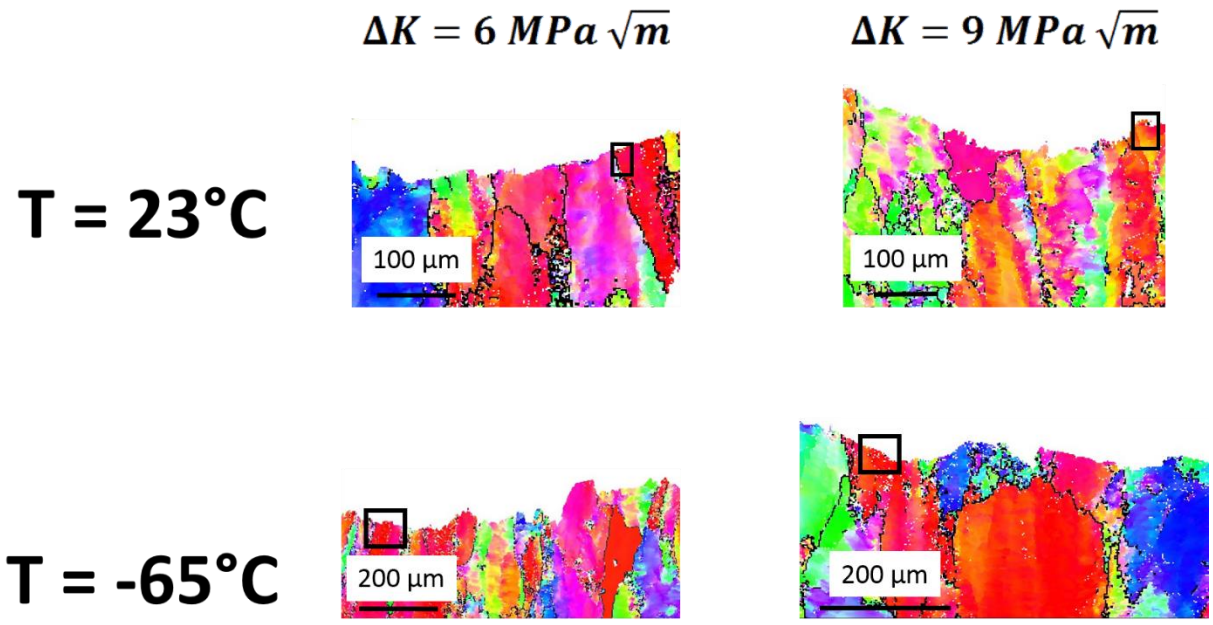

Figure 8 – The global EBSD collected for the four samples taken at ΔK = 6 MPa√m and ΔK = 9 MPa√m for both 23°C and -65°C conditions. The grains selected for HR-EBSD and TEM analysis are highlighted on the EBSD map with a black box.

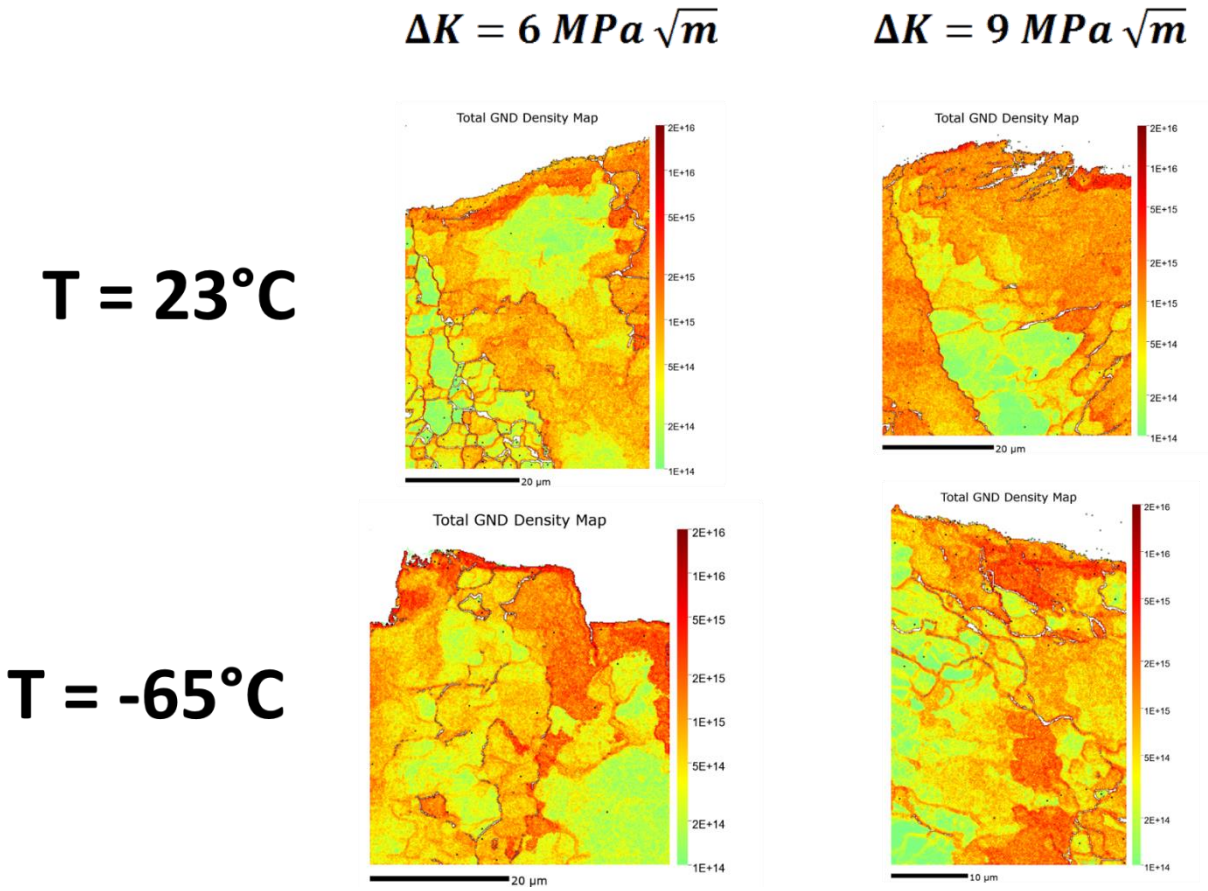

Figure 9 – GND density maps collected for the four samples taken at ΔK = 6 MPa√m and ΔK = 9 MPa√m for both 23°C and -65°C conditions.

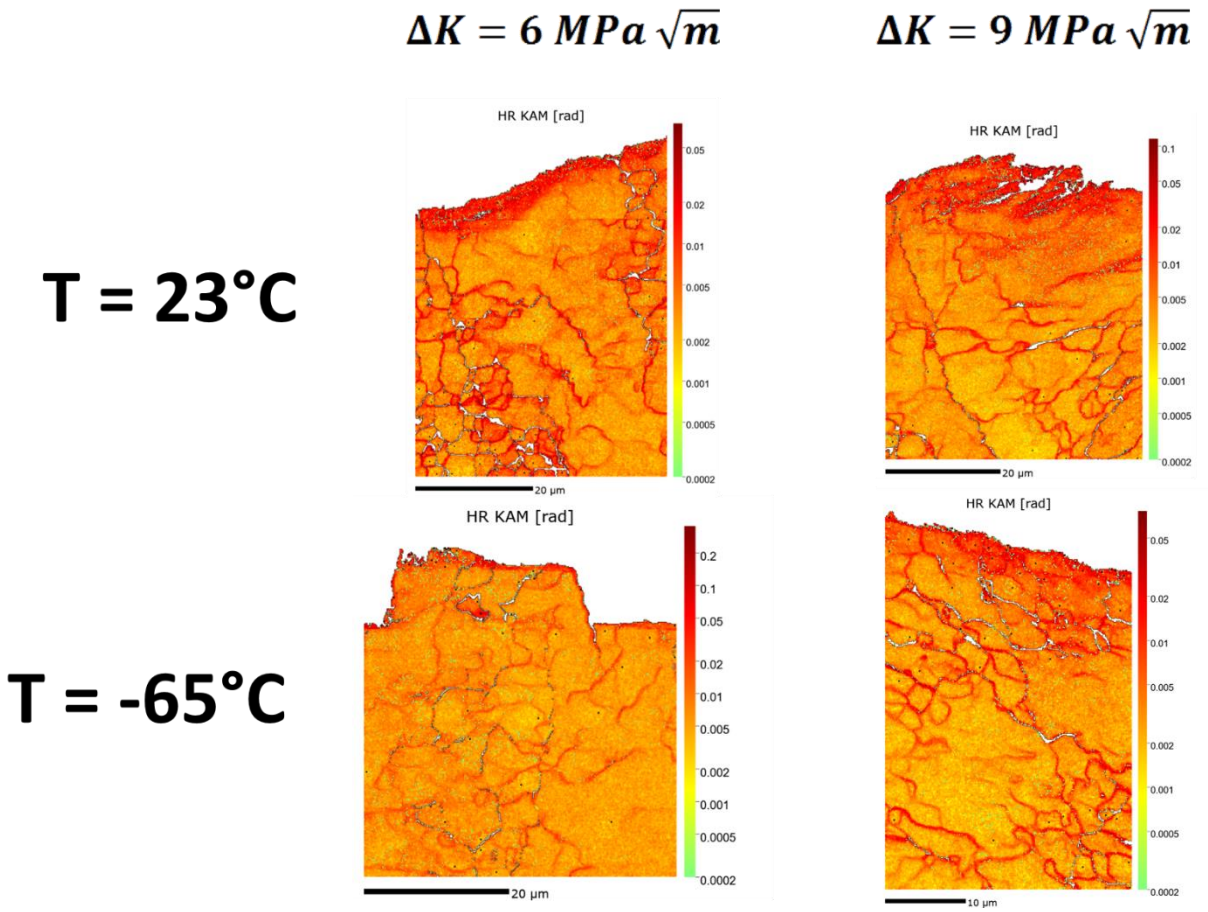

Figure 10 – KAM maps collected for the four samples taken at ΔK = 6 MPa√m and ΔK = 9 MPa√m for both 23°C and -65°C conditions.

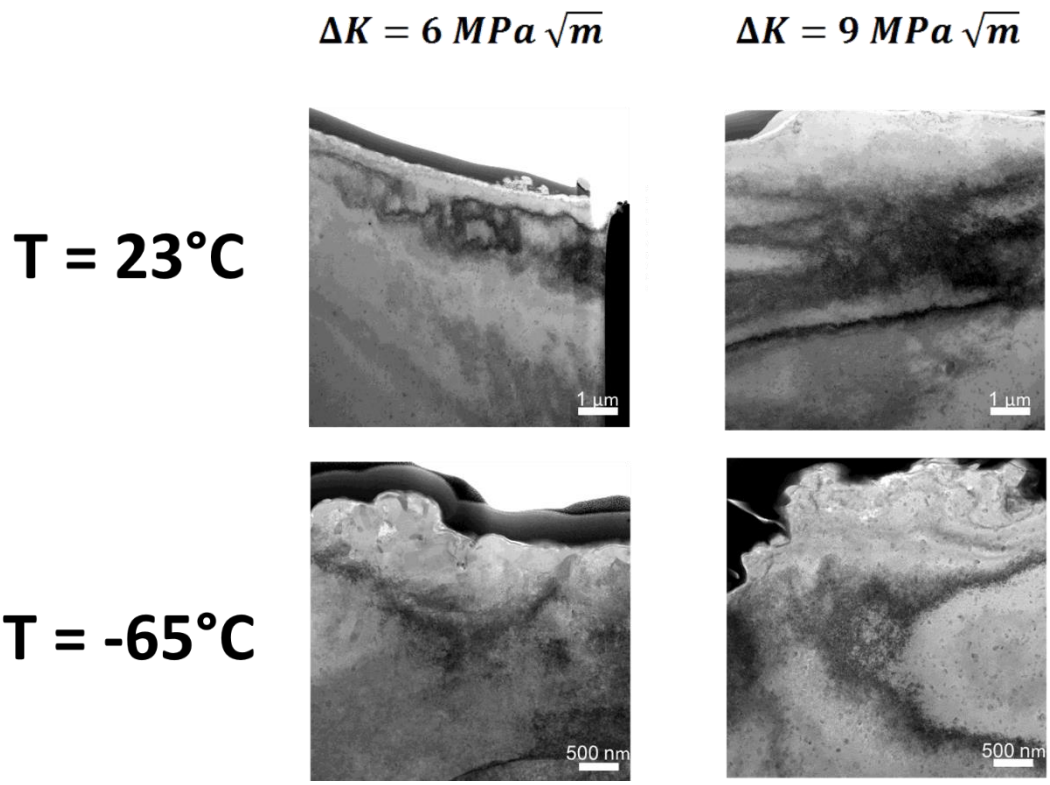

Figure 11 - BF-STEM images collected for the four samples taken at ΔK = 6 MPa√m and ΔK = 9 MPa√m for both 23°C and -65°C conditions used to examine the evolution of the dislocation structure from a near-threshold driving force to a Paris regime driving force.

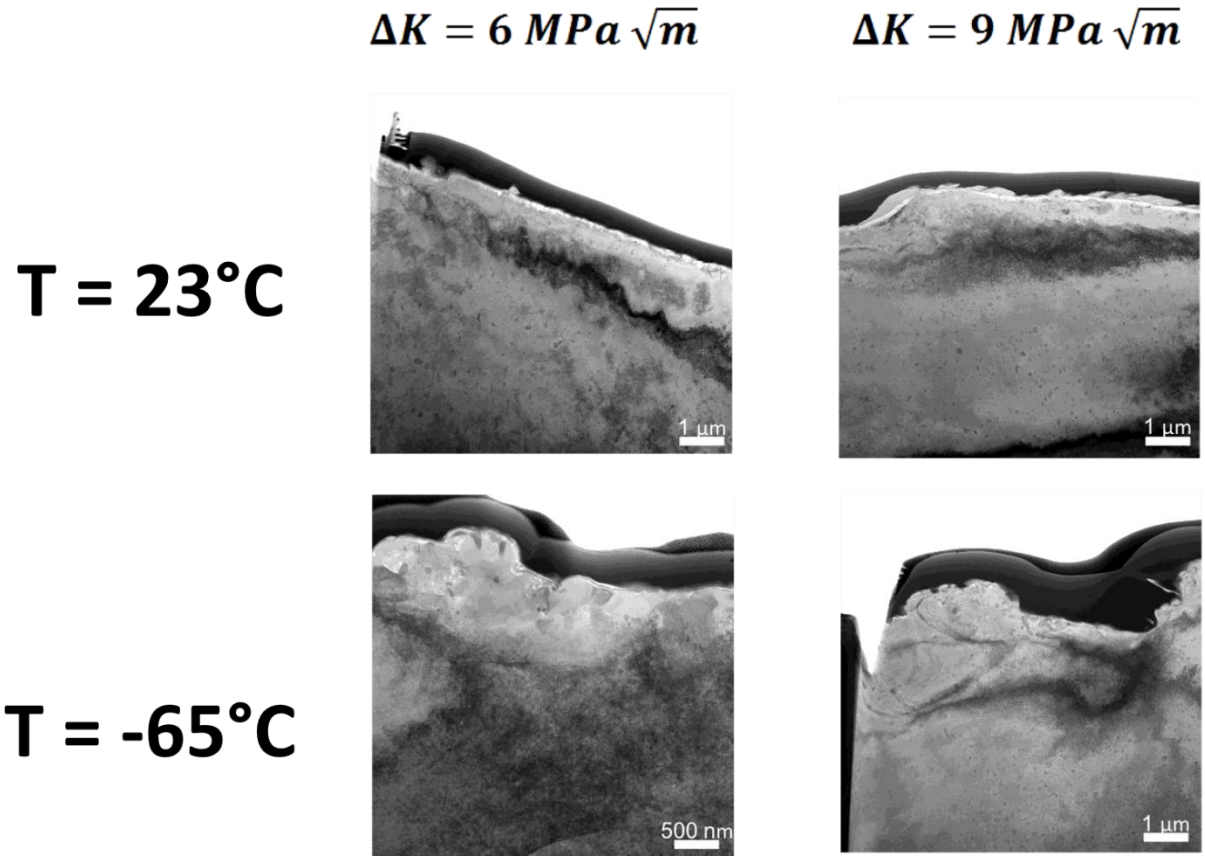

Figure 12 - BF-STEM images collected for the four samples taken at ΔK = 6 MPa√m and ΔK = 9 MPa√m for both 23°C and -65°C conditions used to examine the "recrystallized" layer observed in the TEM samples.

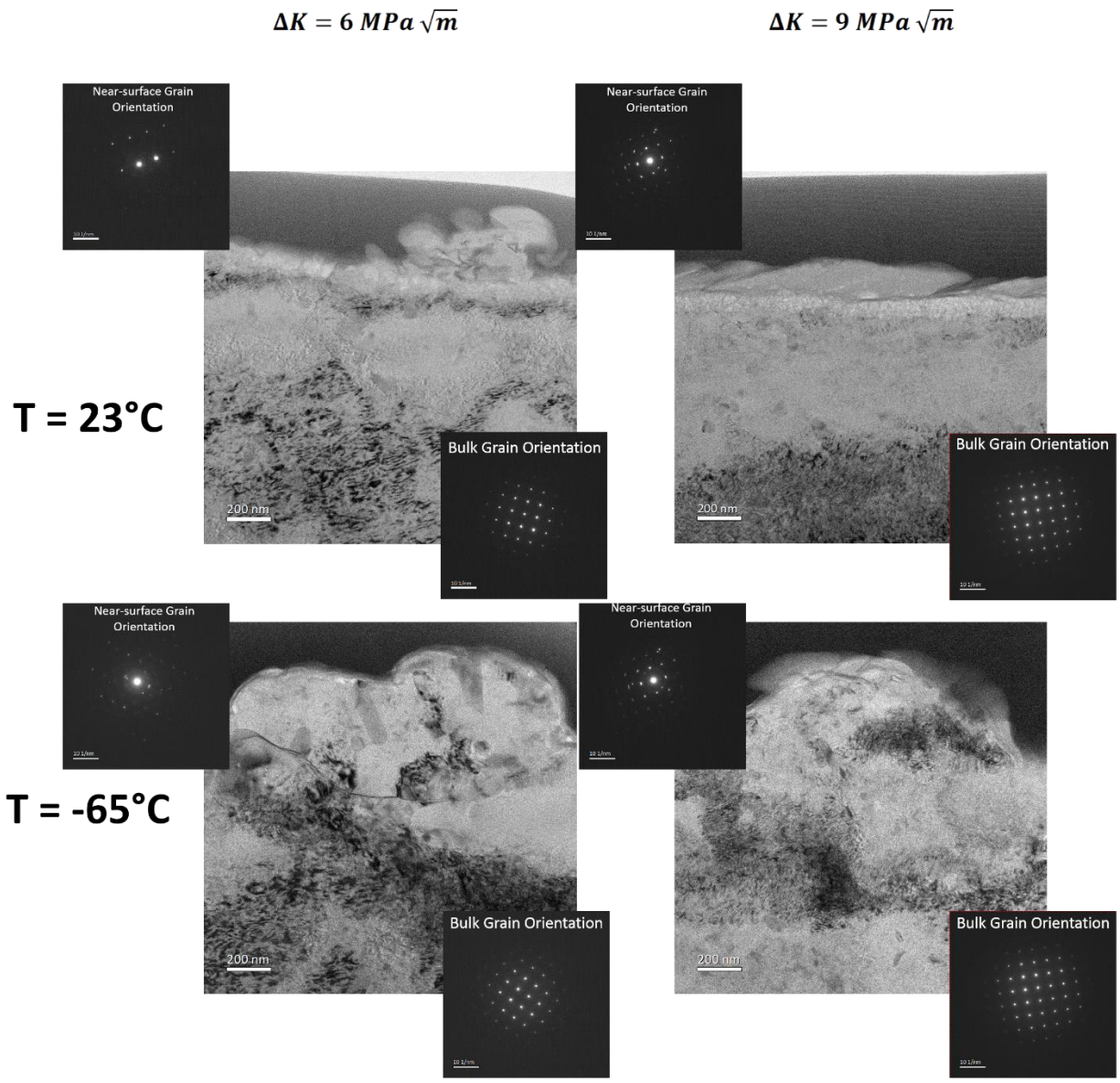

Figure 13 – Diffraction analysis via TEM collected for the four samples taken at ΔK = 6 MPa√m and ΔK = 9 MPa√m for both 23°C and -65°C conditions.

References:

1. Mouritz, A. P. *Introduction to Aerospace Materials*. (Woodhead Publishing, 2012).
2. Suresh, S. *Fatigue of materials*. (Cambridge University Press, 1991).
3. Pook, L. *Metal Fatigue What It Is, Why It Matters*. (Springer, 2007).
4. Ewalds, H. L. & Wanhill, R. J. H. *Fracture Mechanics*. (E. Arnold, 1984).
5. de Jonge, J. B. & Spiekhout, D. J. Use of AIDS Recorded Data for Assesing Service Load Experience. in *Service Fatigue Loads Monitoring, Simulation, and Analysis* 48–66 (1979).
6. Burns, J. T. *et al.* Effect of water vapor pressure on fatigue crack growth in Al – Zn – Cu – Mg over wide-range stress intensity factor loading. *Eng. Fract. Mech.* **137**, 34–55 (2015).
7. Ro, Y., Agnew, S. R. & Gangloff, R. P. Effect of environment on fatigue crack wake dislocation structure in Al-Cu-Mg. *Metall. Mater. Trans. A Phys. Metall. Mater. Sci.* **43**, 2275–2292 (2012).
8. Burns, J. T. *et al.* Effect of water vapor pressure on fatigue crack growth in Al-Zn-Cu-Mg over wide-range stress intensity factor loading. *Eng. Fract. Mech.* **137**, 34–55 (2014).
9. Stanzl, S. E., Mayer, H. R. & Tschegg, E. K. The influence of air humidity on near-threshold fatigue crack growth of 2024-T3 aluminum alloy. *Mater. Sci. Eng. A* **147**, 45–54 (1991).
10. Pao, P. S., Gao, M. & Wei, R. P. Environmentally assisted fatigue-crack growth in 7075 and 7050 aluminum alloys. *Scr. Metall.* **19**, 265–270 (1985).
11. Bonakdar, A., Wang, F., Williams, J. J. & Chawla, N. Environmental Effects on Fatigue Crack Growth in 7075 Aluminum Alloy. *Fatigue Mater. Adv. Emergences Underst.* **43**, 29–41 (2010).
12. Burns, J. T. & Gangloff, R. P. Effect of Low Temperature on Fatigue Crack Formation and Microstructure-Scale Growth from Corrosion Damage in Al-Zn-Mg-Cu. *Metall. Mater. Trans. A* **44**, 2083–2105 (2013).
13. Burns, J. T., Jones, J. J., Thompson, A. W. & Locke, J. S. (Warner. Fatigue crack propagation of aerospace aluminum alloy 7075-T651 in high altitude environments. *Int. J. Fatigue* **106**, 196–207 (2018).
14. Verkin, B. I., Grinberg, N. M., Serdyuk, V. A. & Yakovenko, L. F. Low temperature fatigue fracture of metals and alloys. *Mater. Sci. Eng.* **58**, 145–168 (1983).
15. Moreto, J. *et al.* Environmentally-assisted Fatigue Crack Growth in AA7050-T73511 Al Alloy and AA2050-T84 Al-Cu-Li Alloy. *Mater. Res.* **18**, (2015).
16. Gasquères, C., Sarrazin-Baudoux, C., Petit, J. & Dumont, D. Fatigue crack propagation in an aluminium alloy at 223 K. *Scr. Mater.* **53**, 1333–1337 (2005).
17. Abelkis, P., Harmon, M., Hayman, E., Mackay, T. & Orlando, J. Low Temperature and Loading Frequency Effects on Crack Growth and Fracture Toughness of 2024 and 7475 Aluminum. *Fatigue Low Temp.* 257-257–17 (2008). doi:10.1520/stp32760s
18. Robertson, I. A. N. M. *et al.* Hydrogen Embrittlement Understood. (2015). doi:10.1007/s11663-015-0325-y
19. Robertson, I. M. The effect of hydrogen on dislocation dynamics. *Eng. Fract. Mech.* **65**, 671–692 (2001).
20. Wilkinson, A. J. & Randman, D. Determination of elastic strain fields and geometrically necessary dislocation distribution near nanoindents using electron back scatter diffraction. *Philos. Mag.* **90**, 1159–1177 (2010).
21. Clayburn, Z. BYU OpenXY. Available at: https://github.com/BYU-

MicrostructureOfMaterials/OpenXY.
22. Rhodes, C. G., Mahoney, M. W., Bingel, W. H., Spurling, R. a. & Bampton, C. C. Effects of friction stir welding on microstructure of 7075 aluminum. *Scr. Mater.* **36**, 69–75 (1997).
23. Wert, J. A., Huang, X., Winther, G., Pantleon, W. & Poulsen, H. F. Revealing deformation microstructures A variety of features broadly classed as deformation microstructure. *Mater. Today* **10**, 24–32 (2007).
24. Martin, M. L., Sofronis, P., Robertson, I. M., Awane, T. & Murakami, Y. A microstructural based understanding of hydrogen-enhanced fatigue of stainless steels. *Int. J. Fatigue* **57**, 28–36 (2013).
25. Martin, M. L. A New Approach to Discovering the Fundamental Mechanisms of Hydrogen Failure. (University of Illinois at Urbana-Champaign, 2013).
26. Chandler, C. (FEI) & Megorden, M. (FEI). Platinum Deposition Technical Note. 52 (2007).
27. Arey, B. W. *et al.* Advantages of using Plasma FIB Over a Gallium LMIS Source. *Microsc. Microanal.* **21**, 2001–2002 (2015).
28. Thompson, A. W., Harris, Z. D. & Burns, J. T. Examination of focused ion beam-induced damage during platinum deposition in the near-surface region of an aerospace aluminum alloy. *Micron* **118**, (2019).